# Supporting Documents:
# Distinct spin-lattice and spin-phonon interactions in monolayer magnetic $CrI_3$

Lucas Webster, Liangbo Liang, and Jia-An Yan

## 1. Atomic structures in PBE

Structural parameters calculated using PBE are listed in Table S1.

TABLE S1. Total energy $E_t$ (in eV/cell), optimized lattice constant $a_0$ (in Å), bond length $l$ (in Å), bond angle $\theta_1$ and $\theta_2$, and the energy band gap $E_g$ (in eV) for monolayer $CrI_3$ in NM, AFM, and FM phases calculated using PBE with and without SOC.

| | NM | AFM | | FM | | Exp. |
|---|---|---|---|---|---|---|
| | PBE | PBE | PBE-SOC | PBE | PBE-SOC | bulk [S1] |
| $E_t$ | -28.377 | -31.453 | -32.282 | -31.488 | -32.319 | |
| $a_0$ | 6.988 | 6.999 | 7.007 | 6.999 | 7.008 | 6.867 |
| $l$ | 2.670 | 2.734 | 2.738 | 2.735 | 2.740 | 2.725 |
| $\theta_1$ | 81.86° | 90.4° | 90.4° | 90.6° | 90.6° | |
| $\theta_2$ | 169.2° | 172.8° | 172.8° | 173.2° | 173.3° | |
| $E_g$ | - | 1.263 | 1.024 | 1.132 | 0.890 | 1.2 |

Results from both LDA+U and PBE+U calculations (using U = 3 eV for Cr [S2]) for monolayer $CrI_3$ are listed in Table S2 below.

TABLE S2. Total energy $E_t$ (in eV/cell), optimized lattice constant $a_0$ (in Å), bond length $l$ (in Å), bond angle $\theta_1$ and $\theta_2$, and the energy band gap $E_g$ (in eV) for monolayer $CrI_3$ in NM, AFM, and FM phases calculated using PBE with and without SOC.

| | AFM | | FM | |
|---|---|---|---|---|
| | LDA+U | PBE+U | LDA+U | PBE+U |
| $E_t$ | -31.597 | -28.051 | -31.635 | -28.109 |
| $a_0$ | 6.74 | 7.07 | 6.75 | 7.08 |
| $l$ | 2.689 | 2.774 | 2.689 | 2.775 |
| $\theta_1$ | 87.4° | 90.1° | 87.2° | 90.5° |
| $\theta_2$ | 175.8° | 173.2° | 176.0° | 173.5° |

## 2. Electronic band dispersions in PBE

The electronic band dispersions for the NM, AFM, and FM phases calculated from PBE are shown in Fig. S1.

## 3. Lattice dynamics in PBE

Listed in Table S3 are the PBE results for the NM, AFM and FM phases, respectively. Unlike LDA, PBE yields non-negative phonon dispersions in monolayer $CrI_3$. We list these data for comparison.

## 4. Raman spectra in PBE

The Raman spectra calculated in PBE are shown in Fig. S3.

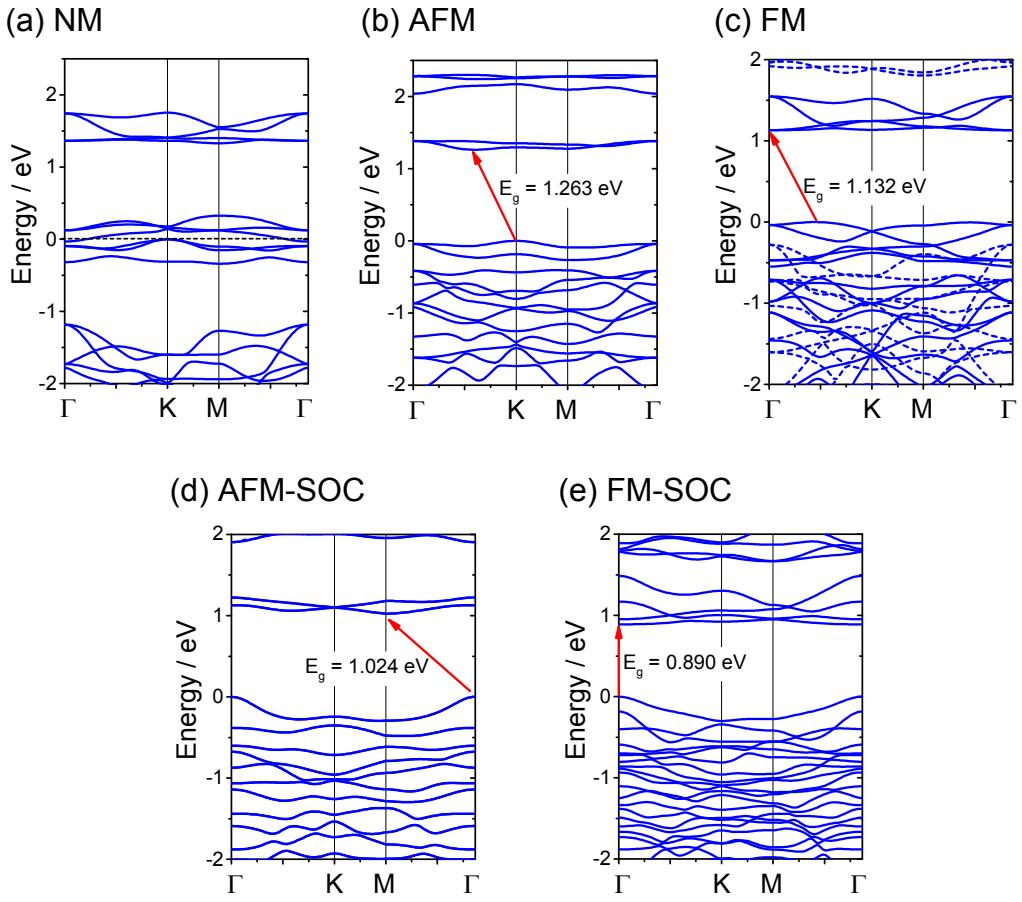


FIG. S1. Electronic band dispersions of monolayer $CrI_3$ calculated using LDA for the NM, AFM, and FM phases, respectively. (a) NM phase; (b) AFM phase without SOC; (c) FM phase without SOC; (d) AFM phase with SOC; (e) FM phase with SOC. In (b) and (c), solid lines denote spin-up while dashed lines denote spin-down bands. The energy band gaps between conduction band minimum (CBM) and valence band maximum (VBM) have been indicated using red arrows in each case. The Fermi level or the VBM has been shifted to zero.

[S1] McGuire, M.A., Dixit, H., Cooper, V.R. and Sales, B.C., 2015. Coupling of crystal structure and magnetism in the layered, ferromagnetic insulator $CrI_3$. Chemistry of Materials, 27(2), pp.612-620.

[S2] Yang, K., Dai, Y. and Huang, B., 2009. Density Functional Characterization of the Electronic Structure and Visible-Light Absorption of Cr-Doped Anatase $TiO_2$, 10, 2327-2333.

TABLE S3. Frequencies of the vibrational modes at Γ calculated using PBE with or without SOC for monolayer $CrI_3$ in NM, AFM, and FM phases, respectively. The Raman active modes have been highlighted in bold. The unit of frequency is in $cm^{-1}$. The symmetries of each mode in the FM phase have been indicated.

| | NM | AFM | | FM | | |
|---|---|---|---|---|---|---|
| Mode No. | PBE | PBE | PBE-SOC | PBE | PBE-SOC | Symmetry |
| 1, 2 | **27.8** | **45.9** | **45.1, 45.2** | **45.7** | **45.3, 45.4** | $E_g$ |
| 3 | 52.1 | 53.8 | 51.1 | 52.1 | 50.9 | $A_{2u}$ |
| 4 | **68.1** | **68.0** | **66.7** | **67.1** | **66.7** | $A_{1g}$ |
| 5, 6 | 84.4 | 73.6 | 72.8, 72.8 | 73.0 | 72.1, 72.2 | $E_u$ |
| 7 | 95.3 | 84.7 | 84.5 | 84.6 | 83.2 | $A_{2g}$ |
| 8, 9 | **87.3** | **93.1** | **92.9, 92.9** | **96.2** | **94.8, 94.9** | $E_g$ |
| 10, 11 | **111.0** | **99.2** | **97.8, 97.9** | **98.9** | **97.7, 98.0** | $E_g$ |
| 12, 13 | 103.0 | 104.3 | 102.8, 102.9 | 103.0 | 101.1, 101.5 | $E_u$ |
| 14 | **125.9** | **117.2** | **115.1** | **119.6** | **117.6** | $A_{1g}$ |
| 15 | 136.5 | 120.2 | 118.8 | 120.2 | 118.3 | $A_{2u}$ |
| 16 | 147.4 | 200.1 | 196.6 | 196.6 | 193.0 | $A_{2g}$ |
| 17, 18 | 211.0 | 208.6 | 206.7, 206.8 | 205.6 | 203.0, 203.1 | $E_u$ |
| 19, 20 | **202.0** | **219.5** | **216.4, 216.4** | **221.0** | **217.4, 217.9** | $E_g$ |
| 21 | 225.6 | 241.8 | 239.1 | 244.8 | 241.0 | $A_{1u}$ |

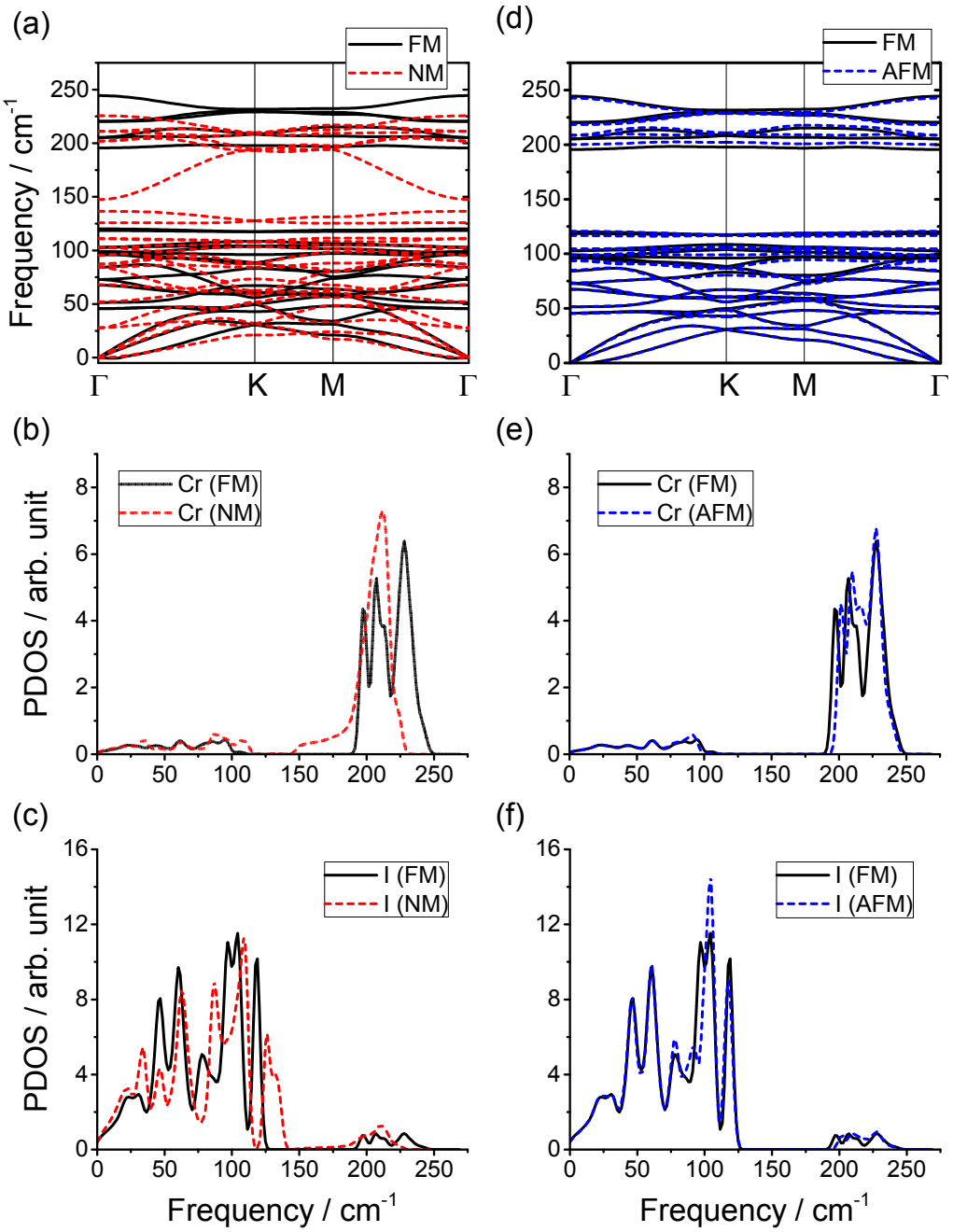


FIG. S2. Phonon band dispersions of monolayer $CrI_3$ calculated using PBE for the NM, AFM and FM phases, respectively. Since FM is the ground state, we have used it as a reference. Left: (a) FM (solid) and NM (dashed); The corresponding partial phonon density of states are shown for two Cr atoms (b) and six I atoms (c), respectively. Right: (d) FM (solid) and AFM (dashed); The corresponding partial phonon density of states are shown for two Cr atoms (e) and six I atoms (f), respectively.

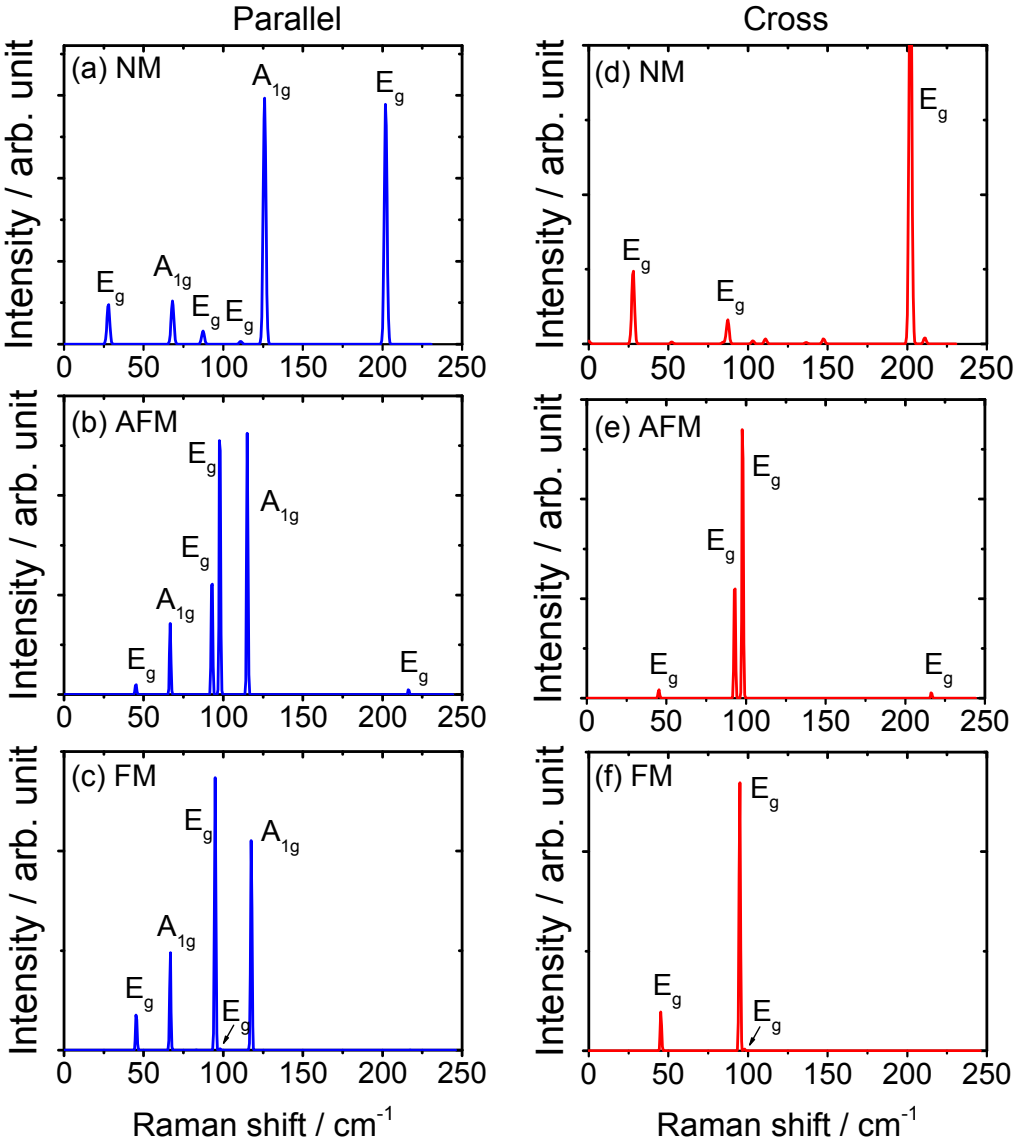


FIG. S3. Polarized Raman spectra for monolayer $CrI_3$ in NM, AFM and FM phases, respectively. Note that since $CrI_3$ in the NM state is metallic, the dielectric tensor for Raman calculations was obtained at a typical experimental laser frequency 1.96 eV (633 nm). Shown on the left are for the parallel polarization laser set-up. On the right are the results with cross laser polarization set-ups. The corresponding mode symmetries for each peak have been indicated. A Gausian broadening with width of 1.0 $cm^{-1}$ has been applied.